

Effect of Nanoparticle Size on Cysteine-Gold Surface Interactions

S. Marzieh Kalantarian, Peter Slovenský, Zhiqiang Wang, Valentin Romanovski, Elena Romanovskaia, Maroš Halama, Michael Auinger, Heng-Yong Nie, and Yolanda S. Hedberg*

Gold nanoparticles (AuNPs) are considered for biomedical applications, and their size influences their effectivity and stability in the human body. This study investigates the interactions between citrate-stabilized AuNPs (5, 10, 15, and 20 nm) and L-Cysteine (Cys). The interactions were probed by time-of-flight secondary ion mass spectrometry (ToF-SIMS), cyclic voltammetry (CV), dynamic light scattering (DLS), and X-ray absorption spectroscopy (XAS). Hydrogenated gold cysteine thiolate molecular ions, gold-sulfur ions, and Au₃^{+/-}, as gold atom representatives, were all detected for the different sizes. Smaller intensity ratios of the gold-cysteine-related peaks versus the gold reference peaks were observed with increasing AuNP size. CV confirmed stronger interactions of smaller AuNPs with Cys. AuNPs bond strongest to the thiol group, followed by the amino group, while no gold-carboxyl interactions were probed. The nonspecific properties of the smallest-sized (5 nm) AuNPs stabilized (less aggregation) by the presence of Cys based on XAS, but all nanoparticle sizes showed more agglomeration in aqueous solution in the presence of Cys based on DLS. The data confirmed that the strength of the binding between AuNPs and Cys is size-dependent, possibly caused by curvature, surface energy, and/or diffusion processes.

1. Introduction

Nanoparticles have extensive applications in nanomedicine owing to their unique characteristics toward high biocompatibility.^[1] In contrast to other nanoparticles, which may show potential toxicity toward normal, healthy human cells, tissues, and organs,^[2] gold nanoparticles (AuNPs) exhibit relatively low toxicity,^[3-7] high stability, high biocompatibility, and good affinity for biomolecules.^[8,9] They can also be synthesized in different sizes, which makes AuNPs widely used or considered for medical applications, such as drug delivery, cancer treatment (using radiation therapy), and imaging cells.^[8,10-13]

The size and shape of the AuNPs are reasonably controllable,^[14,15] which can help to maximize the medical effect.^[13] A 10 or 15 nm nanoparticle includes more than 50 000 gold atoms, which, due to their high density, can improve the transferring

S. M. Kalantarian, P. Slovenský, Z. Wang, Y. S. Hedberg
 Department of Chemistry
 The University of Western Ontario
 London, Ontario N6A 5B7, Canada
 E-mail: yhedberg@uwo.ca

S. M. Kalantarian, P. Slovenský, Z. Wang, Y. S. Hedberg
 Carbon to Metal Coating Institute
 Queen's University
 Kingston, Ontario K7L 3N6, Canada

P. Slovenský, M. Halama
 Technical University of Košice
 Faculty of Materials
 Metallurgy, and Recycling, Institute of Materials
 Košice 042 00, Slovakia

V. Romanovski, E. Romanovskaia
 Department of Materials Science and Engineering
 University of Virginia
 Charlottesville, VA 22904, USA

M. Auinger
 Institute of Chemical Technologies and Analytics
 TU Wien
 Vienna 1060, Austria

M. Auinger
 WMG
 University of Warwick
 Coventry CV4 7AL, UK

H.-Y. Nie, Y. S. Hedberg
 Surface Science Western
 The University of Western Ontario
 London, Ontario N6G 0J3, Canada

H.-Y. Nie
 Department of Physics and Astronomy
 The University of Western Ontario
 London, Ontario N6A 3K7, Canada

The ORCID identification number(s) for the author(s) of this article can be found under <https://doi.org/10.1002/ppsc.202400230>

© 2025 The Author(s). Particle & Particle Systems Characterization published by Wiley-VCH GmbH. This is an open access article under the terms of the [Creative Commons Attribution](https://creativecommons.org/licenses/by/4.0/) License, which permits use, distribution and reproduction in any medium, provided the original work is properly cited.

DOI: 10.1002/ppsc.202400230

productivity in radiation therapy for cancer treatment.^[16,17] One of the common synthesis routes for AuNPs is the citrate method, in which trisodium citrate is used to reduce tetrachloroauric acid.^[15] In this case, citrate acts both as a reducing agent and the surface stabilizer that stabilizes the AuNPs in aqueous solutions via electrostatic repulsion between individual nanoparticles.

The effectiveness, reactivity, and stability of AuNPs in the human body are size-dependent. According to the literature, smaller-sized AuNPs are significantly more reactive (degrading faster) than larger-sized AuNPs.^[18] It has been shown that positively charged nanospheres showed ≈ 10 times higher cellular uptake than either neutral or negatively charged ones.^[19] Also, the cell uptake concentration of rod-shaped AuNPs differs from sphere-shaped AuNPs because of the increase in specific surface area.^[20–22] Overall, AuNP size, alongside other physicochemical properties,^[23–25] can change the AuNPs' interactions with biological systems.

Amino acids, abundantly present in the human body environment, have a high affinity to gold due to their amino group ($-\text{NH}_2$).^[26] L-cysteine (Cys) has a thiol functional group ($-\text{SH}$) in addition to the amino group, which makes it among the most likely amino acids to bind to gold in a physiological environment.^[27–30] A solid-state NMR study revealed that Cys binds to AuNPs in two layers;^[31] the first layer consisted of Cys molecules forming thiolate bonds with the gold surface with their charged amino and carboxyl groups oriented away from the gold surface. The second layer positioned its amino and carboxyl groups toward the first layer, with its sulfur groups facing away. It should be noted that that study was in the solid state, and the orientation of the ligands might be different in an aqueous state. This is why it might be contradicted by a resonance light scattering study claiming that the amino groups of the first layer would interact with negatively charged (citrate-coated) AuNPs, causing self-assembly of the nanoparticles.^[32–34]

Time-of-flight secondary ion mass spectrometry (ToF-SIMS)^[35] is a surface-sensitive technique, that probes elemental and molecular information over the outermost 1–3 nm of the surface.^[36] It is suitable for exploring the surface and interface chemistry of self-assembled monolayers (SAMs), most of which are less than 2.5 nm.^[37,38] An ion (m/z 417) detected by ToF-SIMS was attributed to a complex of threonine-O-3-phosphate and gold, termed as threonine-O-3-phosphate aureate.^[39] It would be intriguing to understand how thiol groups and amino groups compete to interact with Au. In fact, it has been shown that ToF-SIMS peptide signal intensity was enhanced on an enlarged (nanostructured) gold surface, with very good sensitivity for thiol groups.^[40] Therefore, those amino acids containing amino and thiol functional groups, such as Cys, would serve as a model amino acid to compare the interaction between Au and thiol groups versus amino groups.

ToF-SIMS signifies a dynamic instrument within the field of nanotoxicology that is being used for the biomolecular imaging of cell-nanoparticle interactions. It can then evaluate the chemical distribution of amino acids within newly synthesized gold particles. ToF-SIMS collects specific chemical information from the surface with high sensitivity. It can identify the formed com-

plexes/ligands between gold and Cys and, therefore, enable the comparison of the effect of the size of AuNPs on Cys binding or adsorption. Hydrogenated, dehydrogenated, and other Cys and gold-Cys species can be identified through ToF-SIMS.^[35,41–45] It is worth mentioning the unavoidability of sulfur contamination of gold surface due to the extreme affinity of sulfur and gold,^[46] which may be called adventitious sulfur^[47] and is largely manifested by ToF-SIMS thanks to the high ion yields of sulfur-related species (mainly S^- , AuS^- , and Au_3S^-). Fortunately, the intensities of these ions originating from adventitious sulfur are minimal and thus would not impact the ToF-SIMS results when sulfur-containing chemicals^[41,48] are purposely anchored on gold surfaces.

Furthermore, according to our previous studies using ToF-SIMS, a gold cysteine thiolate complex, which is relatively stable, was detected for 5 nm, but not 50 nm, AuNPs. Hence, based on published results, it can be assumed that ToF-SIMS could be used to detect any nanoparticle size effect on the formation of surface complexes and interactions. A stronger Cys-gold interaction for smaller sizes was also detected electrochemically for the same nanoparticles sized 5, 10, 20, and 50 nm.^[48,49]

We hypothesize that the number density (per surface area) and/or strength of Cys-Au bonds is larger for smaller-sized (5, 10 nm) AuNPs than for larger-sized (15, 20 nm) AuNPs. This was investigated for citrate-functionalized AuNPs by ToF-SIMS and cyclic voltammetry (CV). Because size-dependent effects can be influenced by particle agglomeration (including loosely bound particles) and aggregation (altering nanospecific properties), the dry size, hydrodynamic size, and nanospecific properties were furthermore probed by transmission electron microscopy (TEM), dynamic light scattering (DLS), and X-ray absorption spectroscopy (XAS), respectively.

2. Results and Discussion

2.1. Particle Size Distribution and Morphology

The size distributions of the four different AuNPs were distinct, with only a small overlap of the 5 and 10 nm and the 15 and 20 nm AuNPs, respectively, **Figure 1**. All mean sizes were within the nominal size except for the 10 nm, with a slightly smaller (7.4 ± 1.0 nm) mean size. The shape of these AuNPs was spherical, similar to literature findings for citrate-coated AuNPs.^[50–53] There were more particle-particle interactions (aggregation) visible as the size decreased, **Figure 1**.

Nanoparticles will aggregate when there is an imbalance between repulsive electrostatic forces and attractive London-van der Waals forces.^[54,55] According to the Derjaguin, Landau, Verwey, and Overbeek (DLVO) theory, when attractive van der Waals forces outweigh repulsive electrostatic forces, the sum of these forces leads to the total interaction potential between two AuNPs.^[56] This electrostatic repulsion potential can be expressed in different ways depending on the particle size and the double-layer thickness, which depends on the ionic strength.^[57] Based on the DLVO theory, a decrease in the interaction energy barriers is expected as the size decreases in particles. In the same manner, due to the smaller energy barrier, smaller-sized NPs will aggregate more.^[58,59]

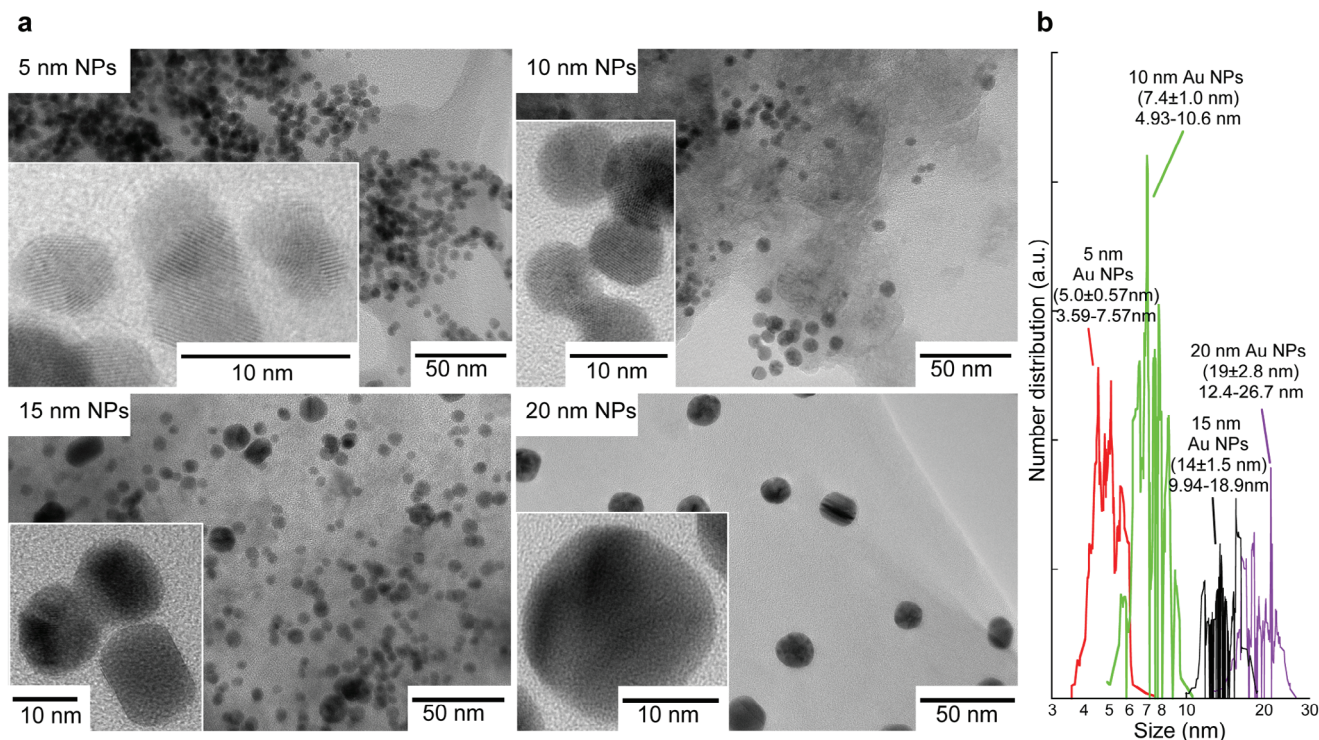


Figure 1. a) TEM images for the 5, 10, 15, and 20 nm AuNPs at different magnifications, and b) number size distribution based on the TEM image evaluations (129–208 individual particles for each AuNPs suspension) with corresponding mean size, standard deviation, minimum, and maximum size.

2.2. Dynamic Light Scattering (DLS)

The mean intensity of DLS increased with increasing nanoparticle size, Figure S1 and Table S1 (Supporting Information). All AuNPs revealed larger mean diameter values than their nominal values in MES+NaCl, indicative of some agglomeration. It should be noted that the smallest nanoparticles (especially 5 and 10 nm) are difficult to detect by DLS, and their mean intensity was close to or below the threshold value for reliable data (indicated with a red dashed line in Figure S1b, Supporting Information). However, the mean intensity increased for all nanoparticle sizes in the presence of Cys except for 15 nm. In all, the presence of Cys likely increased the hydrodynamic size and tendency to agglomerate in solution for all AuNPs sizes. Whether this agglomeration influenced any nonspecific binding is discussed in sections 3.5–3.7. In the next two sections, the results of nanospecific binding are presented and discussed.

2.3. ToF-SIMS

Hydrogenated gold cysteine thiolate molecular ion ($\text{AuSC}_3\text{H}_7\text{NO}_2^+$, m/z 317.99) was studied along with other ions including Au_3^+ m/z 590.89, Au_2S^+ m/z 425.99, and Au_3S^+ m/z 622.96 in the positive mode, and Au_3^- m/z 590.89, AuS^- m/z 229.03, and S^- m/z 32.06, in the negative mode. All ions were normalized toward the total intensity while some specific fragments, as indicated in figure captions, were also normalized toward gold ions representatives

$\text{Au}_3^{-/+}$, to account for differences in AuNPs coverage in the imaged areas.

Figure 2 shows images of S^- , AuS^- and Au_3^- represented by false colors red, green, and blue, respectively, as well as their overlay, for the various sizes of AuNPs. Gold-thiol binding is represented by AuS^- which reveals a much brighter, distinctive map for smaller AuNPs. Both S^- and AuS^- were detected from AuNPs without the presence of Cys, which is due to sulfur contamination that only could be removed using UV/ozone treatment followed by de-ionized water rinse.^[60] It is clearly demonstrated in Figure 2 that these two ions became much stronger after the Cys treatment, reflecting the presence of Cys and its reaction with the AuNPs.

For all AuNP sizes, Au_3^- was detectable, although its intensity was strongest for the smallest (5 nm) AuNPs due to them remaining preferentially in the folded Al foil. With increasing particle sizes, the detected gold signals decreased but were still detectable. The ion images of 5 nm AuNPs show that the deposition and detection of AuNPs were successful. The reason for using Au_3^- as the gold representative and not Au^- (m/z 196.97), despite having a stronger peak, is that Au^- can interfere with $\text{Al}_3\text{H}_4\text{O}_7^-$ (m/z 196.94), which forms on the Al substrate. Au_3^- is known to be the second most intense ion fragment of gold.^[61,62] From Figure 2, it is furthermore clear that AuS^- signals co-locate with Au_3^- signals for the 5 and 10 nm AuNPs but not very much for the 15 and 20 nm AuNPs.^[41]

Ion images of $\text{AuSC}_3\text{H}_7\text{NO}_2^+$ and Au_3^+ for 5 and 20 nm AuNPs are shown in Figure S2 (Supporting Information). They revealed the co-location of these two ions for both AuNP sizes,

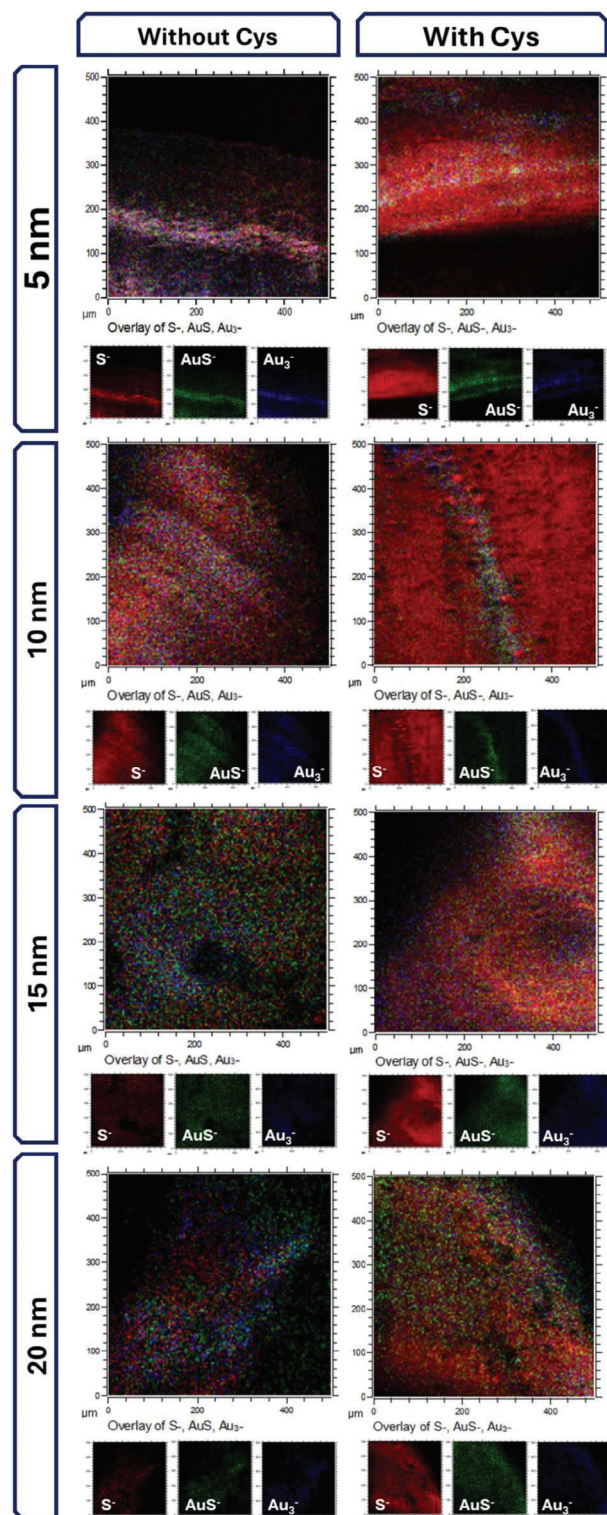


Figure 2. Images of S^- (represented by red), AuS^- (green), and Au_3^- (blue), and their overlay, of the rinsed 5, 10, 15, and 20 nm AuNPs loaded Al foil before (without Cys) and after (with Cys) immersion in a 0.5 mM Cys solution for 24 h. The ion images are presented in false color scales, where a brighter color represents a higher ion intensity.

Figure S2 (Supporting Information). The corresponding spectra, normalized on the Au_3^+ intensity, are shown in Figure S3 (Supporting Information). However, the spectra of $AuSC_3H_7NO_2^+$ were detected but were too weak to draw conclusions about the side effects of the particles because of interfering peaks and a low signal-to-noise ratio, Figure S3 (Supporting Information).

From both the positive ion maps (Figure 2; Figure S2, Supporting Information), it can be concluded that gold signals co-locate with signals originating from sulfur S^- and gold-sulfur AuS^- , or the gold-cysteine fragment $AuSC_3H_7NO_2^+$.

Figure 3a–f show representative spectra of selected regions for Au_3^+ , Au_2S^+ , Au_3S^+ (a–c), and Au_3^- , Au_2S^- , and Au_3S^- (d–f) for the varying AuNPs sizes. $Au_xS^{+/+}$ were investigated to study any evidence of Au-S bonding. All peaks were detectable for all sizes, however, the strongest (when normalized to total or $Au_3^{+/+}$ ion intensities) was seen for the 5 nm AuNPs, followed by increasing AuNP sizes.

Figure 4 presents the intensity of AuS^- (as in Figure 2) normalized over the gold signal (Au_3^-), which gives information on gold-cysteine interactions as a function of the AuNP size directly. Figure 4a shows their spectra for AuS^- for differently sized AuNPs, while Figure 4b shows the averaged ratio for the three different AuNP samples prepared on an Al foil. Figure 4a clearly shows that their intensity, when normalized to the gold signal, is decreasing with increasing AuNPs size. This shows that the interaction between Cys and AuNPs is related to the size of the particles. A stronger interaction could mean stronger or more frequent bonds (of any kind) between gold and Cys.

Likewise, Figure 5 shows the intensities of Au_xS^+ ($x = 2$ and 3) normalized to Au_3^+ intensities. Intensities for Au_xS^+ ($x = 2$ and 3) are decreasing with an increase in AuNPs size.

To investigate if the thiol group interactions were the dominating ones, we also investigated signals relevant to the amino group or carboxylic group of Cys. There was no detectable peak for carboxylic group interactions with gold (AuO^- , $AuCOO^-$, and $AuCOOH^-$). Figure 6a–c shows representative spectra of selected regions for Au_2S^+ , Au_3S^+ , and $AuCN^-$, all normalized to corresponding gold peaks, for the smallest and the largest sizes of AuNPs. To rule out any possible effect of background contamination, similar measurements were also conducted without exposure to Cys. There was a significantly lower signal in that case for the gold-sulfur peaks, confirming that the detected Au_xS^+ , Figure 6a,b, signals mainly originated from gold-cysteine interactions.

The gold-amino group ($AuCN^-$) is presented in Figure 6c. The signal is relatively high even before Cys exposure but still increases after exposure for the 5 nm AuNPs, showing some interaction. However, the relative increase after exposure to Cys for the Au_xS^+ fragments (Figure 6a,b) is far greater, showing that gold bonds strongest to the thiol group.

2.4. Cyclic Voltammetry (CV)

A similar approach that has been described in detail elsewhere^[49] was used to investigate the electrochemical activities of the 5, 10, 15, and 20 nm AuNPs in an electrolyte with 0.5 mM Cys (pH 4.25) and without Cys (pH 4.76), which is shown in Figure 7.

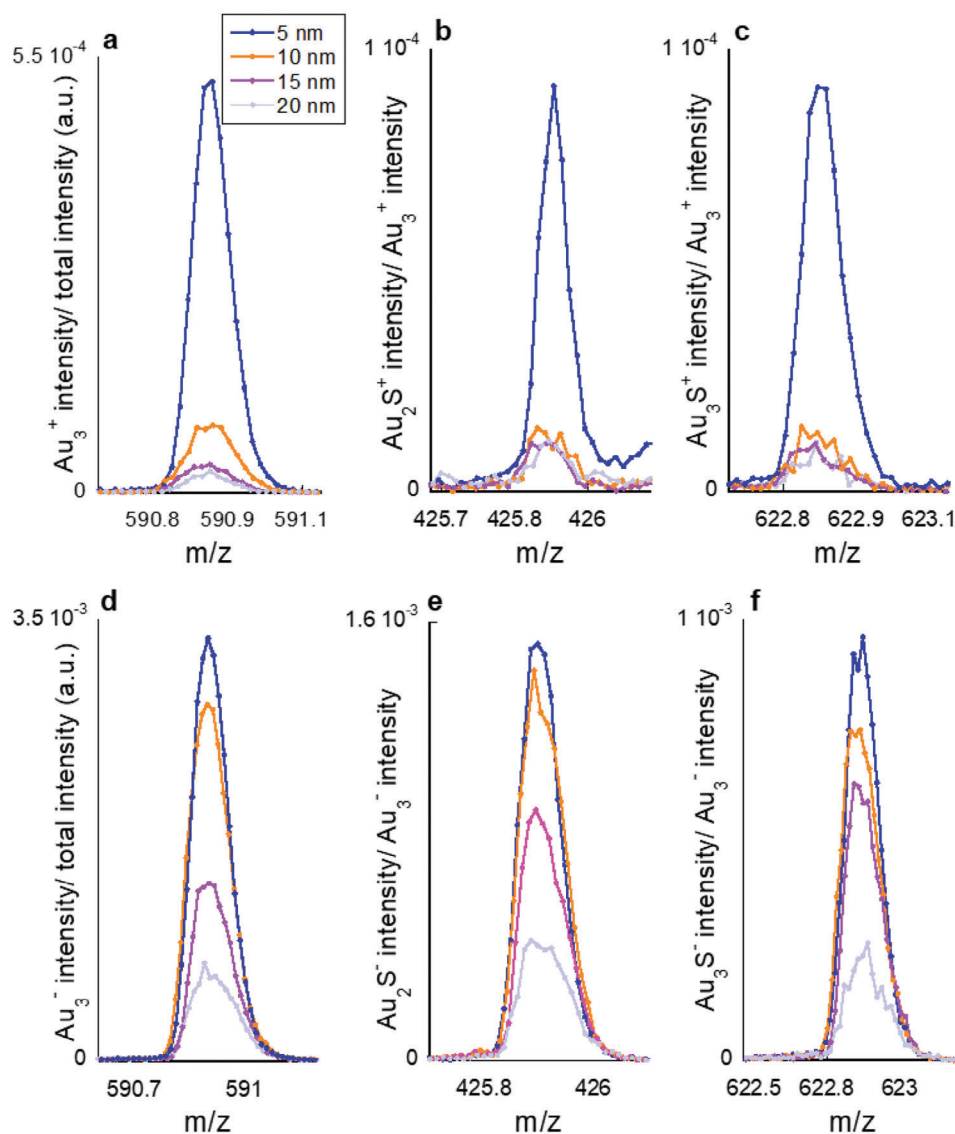


Figure 3. Secondary ion mass spectra representing a) Au_3^+ , b) Au_2S^+ , c) Au_3S^+ , d) Au_3^- , e) Au_2S^- , and f) Au_3S^- for different sizes of AuNPs after exposure to 0.5 mM Cys solution (not pH-adjusted) for 24 h. Representative spectra normalized to total intensity (a and d), Au_3^+ (b and c), and Au_3^- (e and f) are shown. Please note that the lines are only a guide for the eye (connecting raw data) and that the intensity ratios (y-axis scale) vary for each ion.

The electrochemical activity of the AuNPs (at a constant surface area) strongly depended on their size, Figure 7, agreeing with our previous study at pH 7.4 for 5, 10, 20, and 50 nm AuNPs.^[49] In this study, to enable a direct comparison with the ToF-SIMS results, the pH of the solution was much lower (pH 4.25 for Cys-containing solution), so even the larger nanoparticles showed a higher activity.

For particle sizes of 5, 10, and 15 nm AuNPs, repeated measurements confirmed the reproducibility of peak positions and shapes, although the current values were more variable. Current variability may be attributed to the active surface area, which depends on the distribution and dispersity of the AuNPs on the electrode surface. As these are drop-casted on irregularly porous (freshly polished) electrode surfaces, some variability in the distribution of the AuNPs between replicate measurements

is expected. In contrast to the sizes, up to 15 nm, 20 nm-sized AuNPs caused more irreproducible measurements, for which reproducibility was only observed up to the first oxidation peak at $0.78 V_{\text{SCE}}$. However, the second oxidation peak ($\approx 0.9 V_{\text{SCE}}$) exhibited visible splitting and proved challenging to reproduce.

The size dependence was noticeable in several points. The peak position and signal width changed according to the AuNP size. For the 5 nm AuNPs, the first isolated peak was measured at $0.75 \pm 0.002 V_{\text{SCE}}$, corresponding to the oxidation of the amino acid.^[63] This peak shifted only slightly to more positive values for larger sizes (10 nm AuNPs: $0.77 \pm 0.003 V_{\text{SCE}}$, 15 nm AuNPs: $0.76 \pm 0.003 V_{\text{SCE}}$, 20 nm AuNPs: $0.78 \pm 0.003 V_{\text{SCE}}$). A more striking difference among the AuNP sizes was that this amino acid oxidation peak broadened for increasing AuNP size. The second peak ($0.81 \pm 0.003 V_{\text{SCE}}$ for 5 nm, $0.84 \pm 0.002 V_{\text{SCE}}$ for

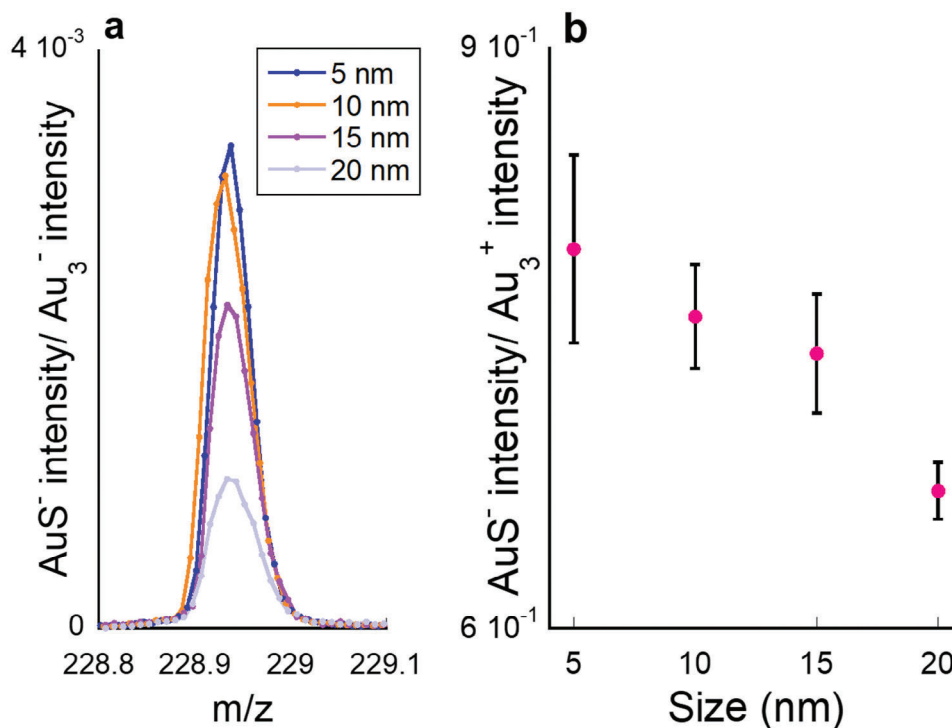


Figure 4. The intensity ratio of AuS⁻ against Au₃⁻ as ion mass spectrum for each of the AuNPs a) and as a function of the size of AuNPs b) after exposure to a 0.5 mM Cys solution for 24 h. The error bars in (b) indicate the standard deviation of three different measured locations representing different AuNPs.

10 nm, $0.87 \pm 0.003 V_{SCE}$ for 15 nm) indicates gold oxidation,^[63,93] with a shifting tendency to more positive values with increasing AuNP size.^[49] For the 20 nm, a splitting tendency for this gold oxidation peak was observed, ranging between the potentials of 0.87 and 0.91 V_{SCE} .

In the CV measurements, we examined the interaction between AuNPs and Cys and interpreted it as an increased presence of free cysteine in solution and decreased Cys-Au interactions for increasing the size of AuNPs, as explained in the following. A plateau peak at 0.4 V_{SCE} ,^[63,93] more significant for the smallest size, is reported to be related to the adsorption of Cys on the gold surface. This plateau peak is not observable for the 20 nm AuNPs, indicative of fewer Cys-gold interactions (except for a large oxidative overpotential). It is well-known that Cys can be oxidized in water.^[64] If there is no direct reaction with gold, water oxidation of Cys can lead to the formation of disulfide bonds or acidic oxidized Cys species; sulfenic acid (R-SOH), sulfinic acid (R-SO₂H), sulfonic acid (R-SO₃H), or cystine (R-S-S-R).^[65] The latter can also adsorb onto the gold surface and cause its surface oxidation.^[66]

The shape of the Cys-related peaks (not only the height) and their position also depend on the Cys concentration.^[67] For the Cys concentration in this study, the shape and position ($0.76 \pm 0.002 V_{SCE}$) agree well with observations in^[67] for the 5 nm AuNPs. The various oxidations involving Cys species may also broaden the peaks. However, for the CV of the 20 nm AuNPs, their broadening of the peak (very broad peak at 0.78 V_{SCE}) suggests the presence of (R-SOH), (R-SO₂H), (R-SO₃H) or (R-S-S-R), where the latter is the dimer Cys. The oxidation poten-

tial of these species (and other disulfide-derived thiol groups) is slightly shifted toward more positive potentials compared to pure Cys.^[30,67]

Fawcett et al.^[63] showed the dependence of gold oxidation (for polycrystalline polished gold) and of the shape of the voltammograms on the concentration of Cys and its species. Our CVs for the 15 and 20 nm AuNP sizes resemble those of Fawcett et al.,^[63] considering expected potential shifts due to different working electrodes. We can, therefore, speculate that slower reactions of Cys with the gold surface of the larger AuNPs, as also seen by ToF-SIMS, could have caused subsequent oxidation to sulfonic acid (peak $\approx 0.78 V_{SCE}$), followed by the reaction with gold (peak at 0.89 V_{SCE}) for the larger sized AuNPs.

The CVs of AuNPs in the absence of Cys showed only one oxidation peak (at $0.81 \pm 0.01 V_{SCE}$ for 5 and 10 nm, $0.86 \pm 0.01 V_{SCE}$ for 15 nm, and $0.89 \pm 0.003 V_{SCE}$ for 20 nm), Figure 7. Hence, with increasing nanoparticle sizes, the oxidation peak maxima shifted slightly to more positive potentials, agreeing with literature findings in a study on 30–120 nm sized AuNPs.^[68,69] This is because smaller AuNPs are more prone to oxidation than larger ones, which leads to a positive shift in the potential with increasing size. In the presence of chloride ions but the absence of Cys, the chlorides effectively hinder the adsorption of hydroxyl ions, thereby impeding the oxidation of gold to AuOH and instead favor binding to chloride. Consequently, under acidic conditions, AuCl₄⁻ species are preferentially formed.^[70]

Overall, without Cys in the solution, there was a significant decrease in current compared to the measurements with Cys in the solution.

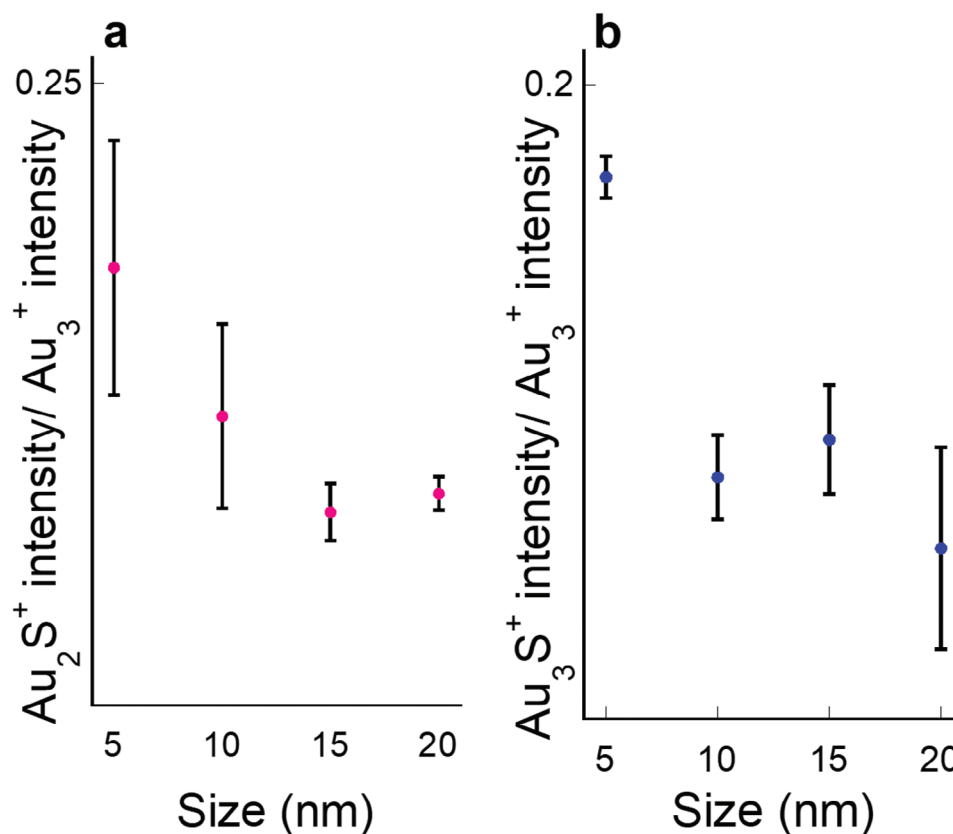


Figure 5. Ion intensity of gold-thiolate ions (Au_xS^+), normalized to Au_3^+ intensities, as a function of AuNPs size (positive ion polarity) after exposure to 0.5 mM Cys for 24 h. The error bars indicate the standard deviation of three different measured locations representing different AuNPs.

When reversing the scan in a solution without Cys, adequate broad reduction peaks were present for all sizes at the same position ($0.55 \pm 0.02 \text{ V}_{\text{SCE}}$). According to,^[71] this peak corresponds to the reduction of Au^{III} to Au^0 (peak position at $0.55 \text{ V}_{\text{SCE}}$ in^[71]). In contrast, in the presence of Cys, there was no or negligible reduction peak due to the irreversible gold-Cys oxidation.^[72–74]

2.5. XAS

Considering the previous sections' findings of more aggregation (dry and in solution) and more binding to Cys for smaller sizes of AuNPs, XAS was utilized to study the electronic structures and nanospecific properties of the differently sized AuNPs as is and after exposure to Cys. This would enable an understanding of whether the observed aggregation for smaller sizes is mitigating the AuNPs' binding to Cys.

There are two main regions in an X-ray absorption spectroscopy spectrum; X-ray absorption near edge structures (XANES) and extended X-ray absorption fine structures (EXAFS). XANES describes the absorption features in the vicinity of an absorption edge up to $\approx 50 \text{ eV}$ above the edge, which is strongly sensitive to the chemistry of the X-ray absorbing atom, such as oxidation state and geometry. In contrast, EXAFS describes the modulation of the absorption coefficient of the element from 50 up to 1000 eV above the absorption edge, which can provide in-

formation on the local structure, such as interatomic distances and coordination numbers.

First, AuNPs were examined independently (without Cys). **Figure 8a** displays the Au L_3 -edge XANES of AuNPs of sizes 5, 10, 15, and 20 nm, and gold foil, which shows an almost identical line shape. A very weak white line (WL) $\approx 11924.5 \text{ eV}$ (Au $2p_{3/2}$ to 5d transition) was observed for all AuNPs and the gold foil because the 5d orbital of gold is fully occupied. It indicates that gold atoms in these AuNPs were in the metallic state, as expected. A closer examination (inset of **Figure 8a**) shows that the WL of all AuNPs was slightly stronger than that of gold foil. WL intensity shows a weak trend of Au foil < 20 nm AuNPs < 15 nm AuNPs < 10 nm AuNPs \approx 5 nm AuNPs. The threshold energy E_0 (the energy of the maximum derivative in **Figure 8b**) of AuNPs was also slightly higher than that of the gold foil. These observations suggest a charge transfer from the Au 5d orbital of AuNPs to surface ligands (citrate).^[75] The Au 5d orbital of AuNPs was not fully occupied (Au 5d depletion due to the interaction between AuNPs and carboxylate groups from citrate); therefore, the excitation of a gold $2p_{3/2}$ electron required slightly more energy. As shown in **Figure 8c,d**, Fourier-transformed EXAFS spectra of AuNPs had a smaller amplitude than the gold foil. Au-Au scattering became weaker as the size of the AuNPs decreased due to a higher surface-to-volume ratio for smaller AuNPs (gold atoms on the surface are less coordinated). In the absence of Cys, the Au-Au peak intensity of 5 nm AuNPs was stronger than that of

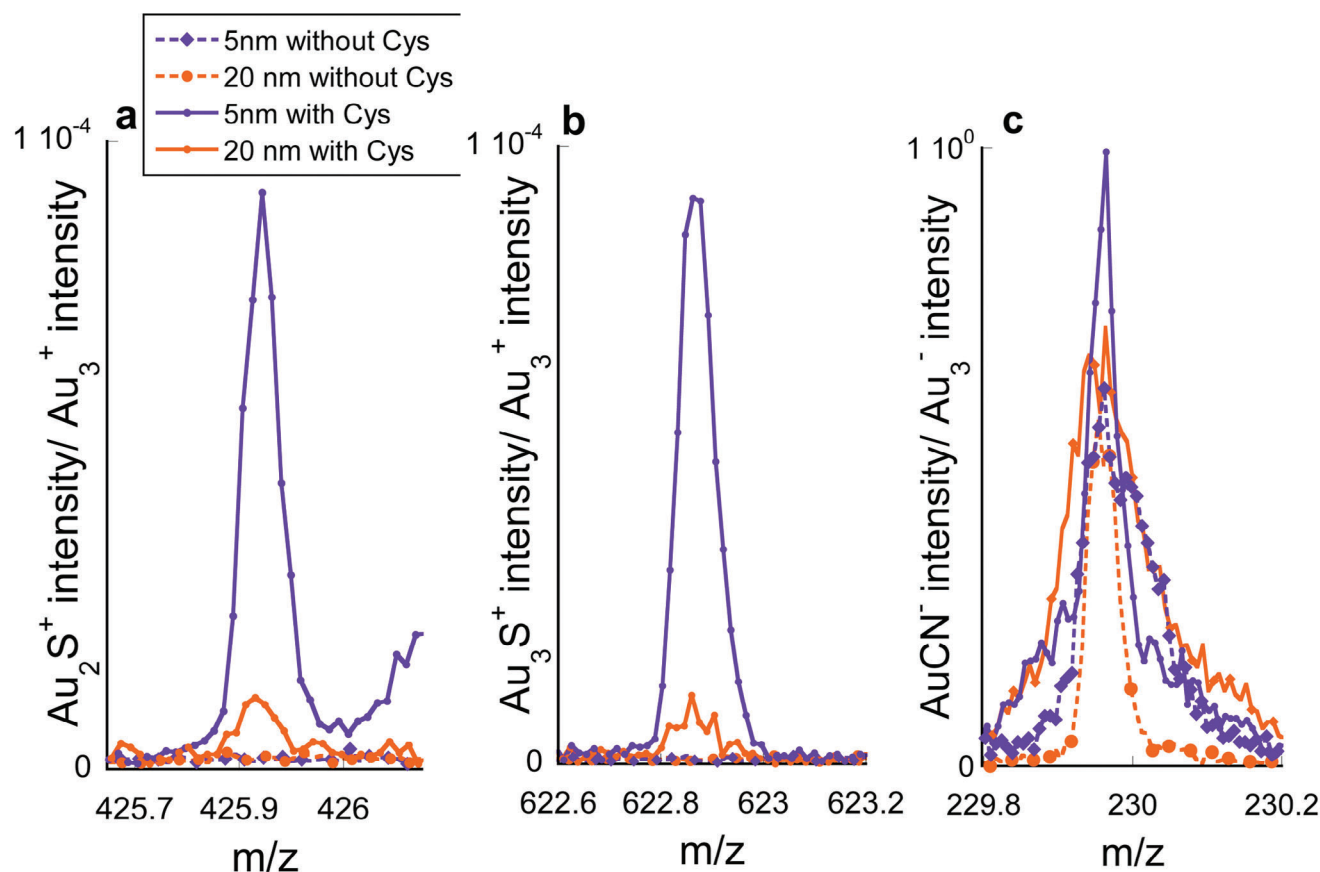


Figure 6. Representative secondary ion mass spectra representing a) Au_2S^+ , b) Au_3S^+ , and c) AuCN^- for 5 and 20 nm AuNPs before (without Cys) and after exposure to 0.5 mM Cys (not pH-adjusted) for 24 h. Representative spectra normalized to total intensity are shown. Please note that the lines are only a guide for the eye (connecting raw data) as the intensity ratios vary for each ion.

10 nm AuNPs but weaker than that of 15 nm AuNPs, suggesting that 5 nm AuNPs were less stable, and aggregation took place.

Figure 9a shows the Au L_3 -edge XANES of AuNPs with Cys in comparison to standard gold foil without Cys. XANES of AuNPs with Cys is similar to their counterpart without Cys. However, in the presence of Cys, the WL intensity shows a more obvious trend with decreasing size of AuNPs; Au foil < 20 nm AuNPs with Cys < 15 nm AuNPs with Cys < 10 nm AuNPs with Cys < 5 nm AuNPs with Cys. The threshold energy E_0 (Figure 9b) of AuNPs with Cys is still slightly higher than that of the gold foil. Fourier-transformed EXAFS spectra of AuNPs with Cys (Figure 9c,d) show that the Au-Au scattering of 5 nm AuNPs with Cys is significantly weaker than that of 10 nm AuNPs with Cys. In the presence of Cys, the Au-Au scattering amplitude decreases with decreasing size of AuNPs. Note that the data for 15 nm AuNPs with Cys (purple curve) is excluded from the discussion due to its poor signal-to-noise ratio and a spike in EXAFS $\approx 6.25 \text{ \AA}^{-1}$ (Figure 8c). Together with the clearer trend in WL intensity, these data suggest that Cys molecules aided in protecting small AuNPs (e.g., 5 nm) from any aggregation, which would result in a change in electronic structure. These smallest AuNP sizes were, therefore, more stable than in the absence of Cys.

2.6. Mechanistic Discussion

This study showed by two independent methods that Cys-gold interactions increase with decreasing AuNPs size (from 20 to 5 nm). CV further indicated that free Cys signals increased with increasing AuNPs size (from 5 to 20 nm). Our hypothesis, that the strength of Cys binding to AuNPs is size-dependent, was confirmed.

According to several studies, a higher surface-to-volume ratio increases reactivity, leading to a reduction of the melting point, depending on the size of particles.^[76] Theoretical predictions suggest that the correlation is significant for particle sizes below 5 nm. As the size of AuNPs decreases, the melting behavior also becomes less uniform, with a broader range of temperatures at which melting occurs. The suppression of melting points was found to be directly correlated with various physicochemical properties, including those important to surface reactivity.^[77] The smaller size also influences the pH gradient in the diffusion layer and, therefore, diffusion distances of Cys to the gold surface,^[78,79] as well as potentially the inner and outer Helmholtz planes. The latter will affect the kinetics of Cys-Au surface reactions beyond a purely transport-controlled effect. This might, hence, shift the

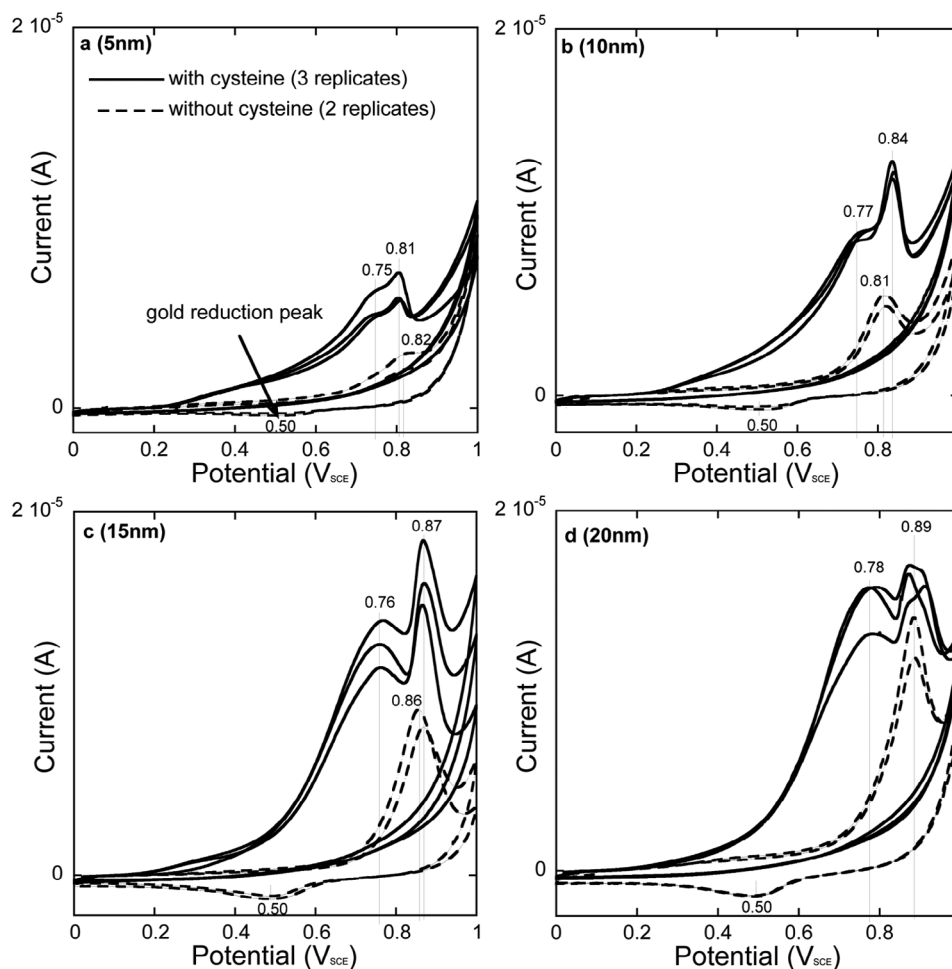


Figure 7. CV (5 mV s^{-1} , OCP to 1 V_{SCE} to OCP) of different sizes (5, 10, 15, and 20 nm) of AuNPs with applied masses corresponding to a constant surface area of $8.64 \times 10^{-2} \text{ cm}^2$, immobilized on a paraffin-impregnated graphite electrode (PIGE), with and without 0.5 mM Cys in 5 mM MES buffer and 5 g L^{-1} NaCl as an electrolyte (not pH-adjusted). The numbers indicate the peak positions for Cys and gold oxidation, as discussed in the text. The solution pH was 4.76 in the absence of Cys and 4.25 in its presence.

CV peaks along the scan direction, especially for stagnant electrolytes (as in this study). It has been suggested previously that diffusion alone cannot explain the higher reactivity of smaller NPs.^[80] Our study also suggests that a difference in diffusion kinetics alone does not explain the higher reactivity of smaller AuNPs toward Cys, as 1) the ToF-SIMS experiments were prepared for 24 h of immersion with excess concentrations of Cys, 2) the difference in CV was not only quantitative but also qualitative, 3) free, unreacted Cys was detected in excess on larger sized AuNP surfaces by CV and 4) our previous modeling study,^[78] which considered diffusion effects, suggested that there should be a linear relationship of Cys-Au reactivity with the reciprocal of the AuNPs size, which is not what this study observed. Therefore, the size dependence most likely involves a clear difference in surface energy. Thermodynamically, it is well understood that the generation of new surface area stores energy ($\sigma \text{ dA}$) which adds to the Gibbs free energy of the gold phase, hence increasing its reactivity.^[80] It has also been shown that decreasing particle size leads to a decrease in the standard molar dissolution Gibbs energy, the standard molar dissolution enthalpy, the standard molar

dissolution entropy, and an increase in the dissolution equilibrium constant.^[81] The higher surface energy of smaller AuNPs also leads to less stability and a higher tendency of aggregation compared to larger ones, which has also been confirmed by TEM and XAS in this study. In the XAS study, the aggregation of the 5 nm compared to the 10 nm AuNPs in the absence of Cys was indicated by a higher occupied density of states on the Au 5d orbital and more coordinated gold atoms in 5 nm AuNPs compared with 10 nm AuNPs. However, in the presence of Cys, the stronger interaction between Cys and the smallest (5 nm) AuNPs effectively prevented their aggregation. Therefore, both Au 5d occupied density of states and coordination showed a clear trend with decreasing AuNP size in the presence of Cys, confirming the AuNPs' nanospecific properties, which were also reflected in the binding studies by ToF-SIMS and CV.

For the spherical AuNPs in this study, the curvature increases strongly with decreasing AuNPs size, which results in a greater conformational degree of freedom for interacting molecules.^[82–84] and a higher packing density. The forces between these materials and their surrounding environment are

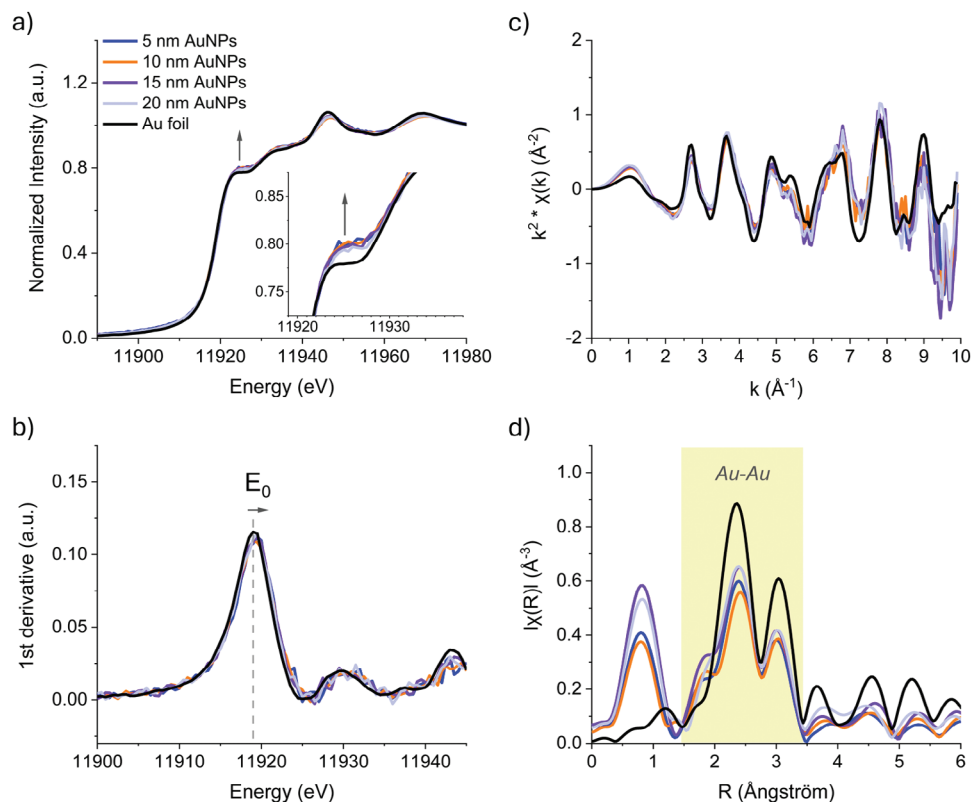


Figure 8. Au L_3 -edge XANES and EXAFS (FY mode) curves of citrate-coated AuNPs (5, 10, 15, and 20 nm) and Au foil. a) XANES, b) the 1st derivative of XANES (threshold energy E_0 is defined as the energy of the maximum derivative of XANES), and k^2 weighted Fourier transforms of EXAFS in c) k space, and d) R space. The inset of a) shows the white line of each AuNP size. The arrows in a) and b) indicate the change in white line intensity and threshold energy of AuNPs compared to standard gold foil, respectively. The color legend in a) corresponds to all figures (a–d).

governed by the interplay of confinement and curvature.^[79] Smaller particles (more curvature) have less prominent packing constraints indicating that thiol coverage per unit area rises as particle size decreases.

Considering that Cys has three functional groups (-COOH, -SH, and -NH₂), it is a promising compound to be used for binding to AuNPs. However, the pKa values are different as it is, 10.28, 8.18, and 1.96 for the amino, thiol, and carboxyl groups, respectively. Among these functional groups, thiol groups demonstrated a higher affinity to gold (as also confirmed in this study) and, therefore, have been widely studied.^[85,86] This is similar to what would be expected in solution for a soft cation like gold or silver, interacting stronger with a thiol group compared with nitrogen and oxygen donors.^[87]

From a geometric aspect, the Cys molecule may not be able to interact with all three functional groups (carboxyl group, amino group, thiol group) when the nanoparticle is small and hence does block a smaller area as compared to large nanoparticles or flat surfaces.^[79,82] This geometric consideration explains well the experimental observation that more free Cys molecules and less or no Cys-Au complexes were detected for larger-sized AuNPs. On top of the pure geometric aspect, the density of surface defects, such as step edges and kinks, might be higher for differently sized AuNPs providing preferential Cys reaction sites. However, it is unclear if this played a role in this study.

2.7. Limitations and Future Studies

The interaction between Cys and the AuNPs is likely influenced by the agent used to stabilize the nanoparticles.^[88] Based on discussions with the supplier and examining the ToF-SIMS spectra, we can conclude that the AuNPs were synthesized using a citrate reduction protocol and they were stored in citrate buffer. No evidence for oxalate, tannic acid, or phosphates was found.

DLS and XAS findings partially contradicted each other, since DLS suggested that the presence of Cys increases agglomeration for all AuNP sizes, while XAS suggested a stabilizing effect of Cys especially for the smallest AuNP size (5 nm). First, 5 nm AuNPs are hard to detect with DLS, so the findings might not be contradicting. Second, DLS measured the hydrodynamic size in situ (in solution), while XAS measured deposited AuNPs after the reaction. This means that DLS could also detect loosely bound particle agglomerates in solution and these might not result in the loss of nanospecific properties. Third, an effect of the Cys solution itself on the detected DLS sizes or in-situ agglomeration behavior cannot be excluded, as also the background solution containing Cys but no AuNPs showed a higher light scattering intensity than the control buffer solution without Cys.

In preparation for the ToF-SIMS measurements, our current approach of removing excessive molecules/ions from the Cys-coated AuNPs deposited on an Al foil is a simple (1 min) rinse using ultrapure water. Insufficient rinses resulted in abundant

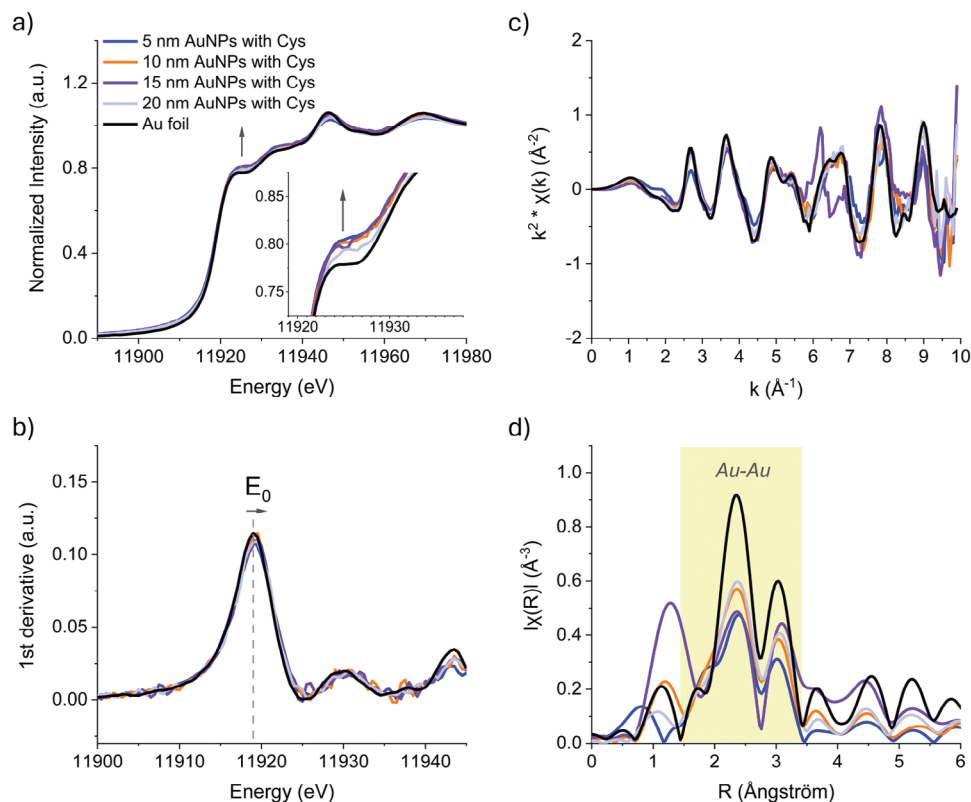


Figure 9. Au L_3 -edge XANES and EXAFS (FY mode) curves of citrate-coated AuNPs (5, 10, 15, and 20 nm) after loading with L-Cys and Au foil. a) XANES, b) the 1st derivative of XANES (threshold energy E_0 is defined as the energy of the maximum derivative of XANES), and k^2 weighted Fourier transforms of EXAFS in c) k space, and d) R space. The inset of a) shows the white line of each AuNP size. The arrows in a) and b) indicate the change in white line intensity and threshold energy of AuNPs compared to standard gold foil, respectively. The color legend in a) corresponds to all figures (a–d).

alkali ion residues (mainly Na^+ and K^+), whose presence apparently reduced the abundance of positive ions related to gold and gold thiolates. However, excessive rinses would remove the AuNPs from the Al foil. Therefore, developing methodologies to rinse off excessive alkali ions while keeping the AuNPs with the molecules of interest adsorbed on a substrate warrants further investigation.

The ion yield of the same species may be different depending on the chemical environment the species is fragmented from, which is the matrix effect in ToF-SIMS.^[40,89] Normalizing intensities of ions of interest against either total ion intensity or the intensity of a specific ion serves to mitigate this matrix effect. This is the reason why $\text{Au}_3^{+/-}$ was used to normalize positive and negative Au-containing ions, respectively, so that the ToF-SIMS results relevant to the interaction between Cys and the differently sized AuNPs can be compared. Hence, we can be confident that our enhanced gold-Cys fragments for smaller AuNPs sizes are due to increased interactions and not a physical effect.

In our work, we performed electrochemical measurements on a very complex system. Changing the size not only changed the reactivity of AuNPs but might also have affected Cys speciation through a different pH profile close to the gold surface when an overpotential is applied.^[78] Future investigations should also determine the effect of pH on the interactions between Cys and AuNPs.

It should be noted that ToF-SIMS is a surface-sensitive method (information depth of $\approx 1\text{--}3$ nm), which is based on mass, so normalization should occur by $\text{Au}_3^{+/-}$ m/z . Larger nanoparticles will be probed only on the surface, whereas smaller nanoparticles have a larger bulk contribution to the signal (2 nm out of a 5 nm nanoparticle is a significant fraction). Still, in all cases, the normalization to the $\text{Au}_3^{+/-}$ signal ensures that only relevant signals from gold surfaces are compared for all different nanoparticle sizes. Note also that the surface area, not the mass, of the differently sized AuNPs was kept constant for the electrochemistry measurements.

3. Conclusion

This study investigated the size dependence of Cys-Au interactions for 5–20 nm AuNPs by two different experimental approaches. Both ToF-SIMS and CV showed stronger and/or more frequent interactions for smaller (5 and 10 nm) than larger (15 and 20 nm) AuNPs with Cys. Free Cys was more detected for larger than smaller NPs by CV. ToF-SIMS studies were conducted for the same mass of 5, 10, 15, and 20 nm AuNPs, pre-reacted with 0.5 mM Cys (in ultrapure water, not pH-adjusted), while CV was conducted in an electrolyte of the same pH and Cys concentration, for equal surface area of AuNPs. ToF-SIMS detected a preferential binding of gold to cysteine through the thiol group, followed by the amino group, and no interactions with

the carboxyl group. Hydrogenated gold thiolate molecular ion, gold, and various gold-sulfur ions were detected for the different sizes of AuNPs. Smaller AuNP sizes revealed stronger peaks for $Au_xS_y^{-/+}$ normalized to $Au_3^{+/-}$. CV revealed these Cys-Au interactions through specific peaks and peak shifts. Free, unreacted Cys (and cystine) showed the opposite – it was increasing with increasing particle size – meaning that the adsorption/bonding with the Au surface weakens for larger NP sizes. The nanospecific properties of the smallest-sized (5 nm) AuNPs were stabilized (less aggregation) by the presence of Cys based on XAS, but all nanoparticle sizes showed more agglomeration in aqueous solution in the presence of Cys based on DLS. In the absence of Cys, the smallest AuNPs aggregated most, based on both TEM and XAS.

4. Experimental Section

Chemicals and Apparatus: 5, 10, 15, and 20 nm citrate-coated AuNPs in aqueous suspension were purchased from Millipore Sigma, Sweden, and Canada (article numbers 741949-25ML, 741957-25ML, 741965-25ML, and 742007-25ML) and stored at 4 °C and vortexed ≈ 10 s before being used. The suspensions had 5.5×10^{13} particles mL^{-1} for 5 nm, 6.0×10^{12} particles mL^{-1} for 10 nm, 1.64×10^{12} particles mL^{-1} for 15 nm, and 6.54×10^{11} particles mL^{-1} for 20 nm AuNPs. If the gold density is assumed to be $19.23 \text{ g } mL^{-1}$, the corresponding mass concentration would be 69.5, 60.6, 55.9, and $52.9 \mu\text{g } mL^{-1}$ for 5, 10, 15, and 20 nm AuNPs stock solutions, respectively. L-cysteine ($\geq 98\%$) was bought from Millipore Sigma, Canada. All the solutions were prepared with ultrapure water (resistivity of $18.2 \text{ M}\Omega \text{ cm}$, Millipore Sigma, Canada). A paraffin-impregnated graphite electrode (PIGE) was manufactured at the Technical University of Košice, Slovakia, through the same process as described elsewhere in detail.^[49]

Time-of-Flight Secondary Ion Mass Spectrometry (ToF-SIMS): For each experimental condition, fresh aluminum (Al) foil was used as a substrate. 80, 92, 99, and 105 μL of the 5, 10, 15, and 20 nm AuNPs suspension (non-diluted), respectively, were dropped on the center of the Al foil surface. The added volumes resulted in the same mass of AuNPs for each size. After being left to dry, each foil was immersed in a 25 mL beaker containing 0.5 mM Cys (not pH-adjusted, with a natural pH of ≈ 4.25) for 24 ± 5 h. After this immersion, the Al foil was left to dry in the air (room temperature). Then, all foils were folded a few times to trap some AuNPs, and the excessive amount of Cys, sodium, potassium, and any possible contamination was rinsed off using ultrapure water for ≈ 60 s. The Al foil folding was found necessary as the AuNPs signal was otherwise too weak, and the prolonged rinsing procedure was necessary to rinse off excess Cys and ions, as ToF-SIMS has only a detection depth of ≈ 2 nm. Rinsing samples for ToF-SIMS analysis is necessary^[91] as it is a highly surface-sensitive method that easily detects contaminants from the solution, which interferes with, or even covers, the surface of interest.

ToF-SIMS (TOF-SIMS IV, ION-TOF GmbH, Germany) was used to study the AuNPs after exposure to Cys solution. In ToF-SIMS, the sample surface was bombarded with a pulsed 25 keV Bi_3^+ primary ion beam for the generation of secondary ions. The secondary ions, extracted with an electric field, flew through a reflectron type of tube and arrived at the detector. The arrival times of ions were converted to mass/charge (m/z) ratios via known species such as hydrogen, carbon, and hydrocarbons. A low-energy electron beam was used to flood the sample for charge compensation. The base pressure of the analysis chamber of the instrument was on the order of 10^{-7} mbar. Secondary ion mass spectra were collected at either 128×128 or 256×256 pixels over the rastered area. Both negative and positive ion spectra were obtained in a mass range of m/z from 0 to 900. The ion mass spectra presented in this study were normalized to the total ion intensity and Au_3^- and Au_3^+ . Negative ion mass spectra were calibrated with CH^- , C_4H^- , and Au_3^- , while positive ion mass spectra were calibrated with CH_3^+ , $C_3H_5^+$, and Au_3^+ . Mass resolutions

for CH^- , C_4H^- , CH_3^+ , and $C_4H_7^+$ were 3000, 4500, 3800, and 5300, respectively. Plotting the intensity of an ion against the pixels generated its image, which was commonly rendered in false color scales with brighter colors representing greater intensities.

In this study, both positive and negative ions were used because information provided by two polarities of ions is often complementary. For example, for gold-sulfur ions, negative ions are much more abundant than their positive counterparts, while the cysteine-gold complex is only fragmented as a positive ion. To account for the heterogeneous distribution of AuNPs on the substrate and to eliminate the “morphology” of the deposition of AuNPs, data of the positive and negative gold-containing ions was normalized against Au_3^+ or Au_3^- , respectively. The normalization is indicated in the captions of the corresponding figure and table. Normalization was necessary because the spectra were acquired from a non-smooth, non-homogeneous surface in different areas, across which the data would not have led to a meaningful comparison without normalization.

It should be highlighted that the Cys fragmentation by ToF-SIMS presented in this study is different than that of SAMs, which has been widely studied by ToF-SIMS before.

Transmission Electron Microscopy (TEM): A JEOL 2100 instrument (Jeol Ltd., Japan) was used for TEM measurements. The AuNPs suspensions were dropped (diluted) from their suspension on the TEM grid, followed by drying. The IMAGEJ software (version 1.52v) was used to quantitatively evaluate the size distribution of 196, 129, 192, and 208 individual particles for the 5, 10, 15, and 20 nm AuNPs, respectively. Data (different images) for the 5, 10, and 20 nm AuNPs used in this study have been published previously.^[48,49] The cumulative size distribution curves were plotted in Origin 2016 and differentiated. The resulting size distribution was smoothed using the adjacent-averaging method with ten points of the window.

Cyclic Voltammetry (CV): To obtain the same surface area for 5, 10, 15, and 20 nm AuNPs, specific volumes (2, 4.6, 7.5, and $10.5 \mu\text{L}$) were drop-cast on the electrode (PIGE) surface using a pipette and left to be dried at room temperature. Then, they were immersed in an electrochemical cell filled with 0.5 mM Cys, $5 \text{ g } L^{-1}$ NaCl (as an electrolyte carrying charge in the solution)^[91] and 5 mM MES as a buffer (pH 4.25). The experiment was done in a three-electrode system using an IviumStat (high power, general purpose potentiostat/galvanostat/ZRA) potentiostat where the PIGE was the working electrode, a platinum wire was the counter electrode, and a saturated (KCl) calomel electrode (SCE) was the reference electrode. The experiment was conducted at a room temperature of 24 °C. The reference electrode was checked against a master electrode prior to each experiment while its cleaning procedure was the same as reported previously.

Open circuit potential (the value after at least 5 min) was the starting potential for all the measurements, followed by scanning (scan rate of $5 \text{ mV } s^{-1}$) toward positive potentials (1 V versus the reference electrode), followed by a negative-going scan to 0 V versus the reference electrode.

Dynamic Light Scattering (DLS): A solution of 5 mM MES buffer containing $5 \text{ g } L^{-1}$ (8.6 mM) NaCl was prepared with and without 0.5 mM Cys. Eight samples were prepared in these solutions containing 50 μL of AuNPs (5, 10, 15, and 20 nm) with the final concentration of (3.48, 3.03, 2.80, and $2.65 \mu\text{g } mL^{-1}$, respectively) and with the final volume of each sample being 1 mL. The samples were not filtered. Additionally, background controls of MES buffer containing NaCl were measured with and without Cys as well. Each sample was analyzed in triplicate using DLS with a Litesizer 500 (Anton Paar) after a 1-minute equilibration period at room temperature. The measurement angle was automatically determined, the quality mode was automatic with a maximum number of runs of 60, and the solvent setting was chosen as NaCl (preset at 1 mM) with the material of interest being gold (refractive index of 1.3307 and 0.6480, respectively, a viscosity of 0.0009558 Paxs).

X-ray Absorption Spectroscopy (XAS): Au L_3 -edge X-ray absorption near edge structures (XANES) and extended X-ray absorption fine structures (EXAFS) spectroscopies of AuNPs (5, 10, 15, and 20 nm) loaded with/without Cys (with the molar ratio (Au/L-Cys) of 7.18, 6.27, 5.78, and 5.46 for 5, 10, 15, and 20 nm AuNPs, respectively) were collected on the HXMA beamline of the Canadian Light Source (CLS). The same amount of each sample was placed on Kapton tape by drop casting. The beamline

energy was calibrated using gold foil as a reference ($E_0 = 11919$ eV). The fluorescence yield (FY) spectrum of each sample was recorded by collecting Au $L\alpha$ X-ray and normalized to the incident photon flux (I_0). XANES and EXAFS spectra were processed using Athena software (version 0.9.26).^[92]

Supporting Information

Supporting Information is available from the Wiley Online Library or from the author.

Acknowledgements

The author would like to acknowledge helpful discussions with Herbert Danning, Vienna University of Technology. This work was supported by the Carbon to Metal Coating Institute (C2MCI) at Queen's University, Kingston, ON, Canada. Part or all of the research described in this paper was performed at the Canadian Light Source, a national research facility of the University of Saskatchewan, which is supported by the Canada Foundation for Innovation (CFI), the Natural Sciences and Engineering Research Council (NSERC), the Canadian Institutes of Health Research (CIHR), the Government of Saskatchewan, and the University of Saskatchewan. The authors would like to acknowledge funding from the Swedish Foundation for Strategic Research (SSF, #FFL18-0173), the Swedish Research Council (VR, #2019-03657), the Wolfe-Western fellowship, Canada (#2020), the Canada Research Chairs Program (CRC-2019-00425), startup funds at Western University, Canada (Dept. Chemistry, 2020), and funding from the New Frontiers in Research Fund, Transformation, Canada (#NFRFT-2020-00573).

Conflict of Interest

The authors declare no conflict of interest.

Author Contributions

The manuscript was written through the contributions of all authors. All authors have given approval to the final version of the manuscript. S.M.K. wrote the original draft and performed ToF-SIMS and DLS measurements and evaluation. P.S. wrote the original draft, performed CV measurements, and evaluated for CV. Z.W. wrote the original draft and performed XAS measurements, evaluation, review, and editing. V.R. performed TEM measurements and evaluation. E.R. performed scientific discussions and review. M.H. performed supervision of CV measurements and discussions. MA did review and editing. HYN performed supervision of ToF-SIMS, review, and editing. Y.S.H. performed conceptualization, project administration, funding acquisition, supervision, evaluation, review, and editing.

Data Availability Statement

The data that support the findings of this study are available from the corresponding author upon reasonable request.

Keywords

cyclic voltammetry, cysteine, DLS, gold nanoparticles, TEM, ToF-SIMS, XAS

Received: October 5, 2024

Revised: January 28, 2025

Published online:

- [1] C. Carnovale, G. Bryant, R. Shukla, V. Bansal, *Prog. Mater. Sci.* **2016**, *83*, 152.
- [2] P. Chen, H. Wang, M. He, B. Chen, B. Yang, B. Hu, *Ecotoxicol. Environ. Saf.* **2019**, *171*, 337.
- [3] Y. Pan, S. Neuss, A. Leifert, M. Fischler, F. Wen, U. Simon, G. Schmid, W. Brandau, W. Jahnen-Dechent, *Small* **2007**, *3*, 1941.
- [4] C. Fernández-Ponce, J. P. Muñoz-Miranda, D. M. de los Santos, E. Aguado, F. García-Cozar, R. Litrán, *J. Nanopart. Res.* **2018**, *20*, 305.
- [5] S. Chaicherd, M. C. Killingsworth, D. Pissuwan, *SN Appl. Sci.* **2019**, *1*, 336.
- [6] U. Carlander, K. Midander, Y. S. Hedberg, G. Johanson, M. Bottai, H. L. Karlsson, *ACS Appl. Bio. Mater.* **2019**, *2*, 1006.
- [7] H. K. Patra, S. Banerjee, U. Chaudhuri, P. Lahiri, A. K. Dasgupta, *Nanomedicine* **2007**, *3*, 111.
- [8] L. Dykman, N. Khlebtsov, *Chem. Soc. Rev.* **2012**, *41*, 2256.
- [9] J. R. Nicol, D. Dixon, J. A. Coulter, *Nanomedicine* **2015**, *10*, 1315.
- [10] M. Y. Kalashgrani, N. Javanmardi, *Adv. Appl. NanoBio-Technol.* **2022**, *3*, 1.
- [11] C. P. Mandhata, C. R. Sahoo, R. N. Padhy, *Biol. Trace Elem. Res.* **2022**, *200*, 5307.
- [12] S. Sargazi, U. Laraib, S. Er, A. Rahdar, M. Hassanisaadi, M. N. Zafar, A. M. Díez-Pascual, M. Bilal, *Nanomaterials* **2022**, *12*, 1102.
- [13] Y. C. Dong, M. Hajfathalian, P. S. N. Maidment, J. C. Hsu, P. C. Naha, S. Si-Mohamed, M. Breuille, J. Kim, P. Chhour, P. Douek, H. I. Litt, D. P. Cormode, *Sci. Rep.* **2019**, *9*, 14912.
- [14] J. Turkevich, *Gold Bull* **1985**, *18*, 86.
- [15] B. John Turkevich, P. Cooper Stevenson, J. Hillier, *Discuss. Faraday Soc.* **1951**, *11*, 55.
- [16] K. Haume, S. Rosa, S. Grellet, M. A. Śmiatek, K. T. Butterworth, A. V. Solov'yov, K. M. Prise, J. Golding, N. J. Mason, *Cancer Nanotechnol.* **2016**, *7*, 8.
- [17] D. Kwatra, A. Venugopal, S. Anant, *Transl. Cancer Res.* **2013**, *2*, 330.
- [18] S. McCarrick, K. Midander, M. Krausová, U. Carlander, H. L. Karlsson, *Int. J. Nanomed.* **2021**, *16*, 5895.
- [19] D. Kumar, I. Mutreja, K. Chitcholtan, P. Sykes, *Nanotechnology* **2017**, *28*, 475101.
- [20] B. D. Chithrani, A. A. Ghazani, W. C. W. Chan, *Nano Lett.* **2006**, *6*, 662.
- [21] B. D. Chithrani, W. C. W. Chan, *Nano Lett.* **2007**, *7*, 1542.
- [22] A. Albanese, W. C. W. Chan, *ACS Nano* **2011**, *5*, 5478.
- [23] E. C. Cho, J. Xie, P. A. Wurm, Y. Xia, *Nano Lett.* **2009**, *9*, 1080.
- [24] T. S. Hauck, A. A. Ghazani, W. C. W. Chan, *Small* **2008**, *4*, 153.
- [25] M. Ferrari, *Nat. Rev. Cancer* **2005**, *5*, 161.
- [26] K. Kudpeng, P. Thiravetyan, *Min. Metall. Explor.* **2021**, *38*, 2185.
- [27] S. Aryal, B. K. C. Remant, N. Dharmaraj, N. Bhattarai, C. H. Kim, H. Y. Kim, *Spectrochim. Acta. A Mol. Biomol. Spectrosc.* **2006**, *63*, 160.
- [28] Y. Zhao, F. Zhou, H. Zhou, H. Su, *Phys. Chem. Chem. Phys.* **2013**, *15*, 1690.
- [29] P. Rodríguez-Zamora, C. A. Cordero-Silis, J. Fabila, J. C. Luque-Ceballos, F. Buendía, A. Heredia-Barbero, I. L. Garzón, *Langmuir* **2022**, *38*, 5418.
- [30] P. K. Sudeep, S. T. S. Joseph, K. G. Thomas, *J. Am. Chem. Soc.* **2005**, *127*, 6516.
- [31] A. Abraham, E. Mihaliuk, B. Kumar, J. Legleiter, T. Gullion, *J. Phys. Chem. C.* **2010**, *114*, 18109.
- [32] A. Mocanu, I. Cernica, G. Tomoaia, L. D. Bobos, O. Horovitz, M. Tomoaia-Cotisel, *Colloids Surf A Physicochem. Eng. Asp.* **2009**, *338*, 93.
- [33] Z. P. Li, X. R. Duan, C. H. Liu, B. A. Du, *Anal. Biochem.* **2006**, *351*, 18.
- [34] A. Majzik, R. Patakfalvi, V. Hornok, I. Dékány, *Gold Bull* **2009**, *42*, 113.
- [35] A. Benninghoven, *Angew. Chem. Int. Ed. Eng.* **1994**, *33*, 1023.
- [36] J. Ekar, P. Panjan, S. Drev, J. Kovač, *J. Am. Soc. Mass Spectrom.* **2022**, *33*, 31.
- [37] A. Shaheen, J. M. Sturm, R. Ricciardi, J. Huskens, C. J. Lee, F. Bijkerk, *Langmuir* **2017**, *33*, 6419.

- [38] C. L. Yeung, S. Charlesworth, P. Iqbal, J. Bowen, J. A. Preece, P. M. Mendes, *Phys. Chem. Chem. Phys.* **2013**, *15*, 11014.
- [39] A. V. Singh, H. Jungnickel, L. Leibrock, J. Tentschert, P. Reichardt, A. Katz, P. Laux, A. Luch, *Sci. Rep.* **2020**, *10*, 261.
- [40] Y. P. Kim, T. G. Lee, *Anal. Chem.* **2012**, *84*, 4784.
- [41] G. J. Leggett, M. C. Davies, D. E. Jackson, S. J. B. Tendler, *Phys. Chem.* **1993**, *97*, 5348.
- [42] V. Secchi, G. Iucci, M. Dettin, A. Zamuner, S. De Rosa, L. Tortora, C. Battocchio, *Langmuir* **2019**, *35*, 16593.
- [43] H. Y. Nie, *Anal. Chem.* **2010**, *82*, 3371.
- [44] J. C. Vickerman, N. Winograd, *Int. J. Mass Spectrom.* **2015**, *377*, 568.
- [45] B. Simões, W. J. Guedens, C. Keene, K. Kubiak-Ossowska, P. Mulheran, A. M. Kotowska, D. J. Scurr, M. R. Alexander, A. Broisat, S. Johnson, S. Muyldermans, N. Devoogdt, P. Adriaenssens, P. M. Mendes, *ACS Appl. Mater. Interfaces* **2021**, *13*, 17353.
- [46] G. Chen, *Comput. Theor. Chem.* **2021**, *1195*, 113094.
- [47] O. Einsle, D. C. Rees, *Chem. Rev.* **2020**, *120*, 4969.
- [48] H.-Y. Nie, E. Romanovskaia, V. Romanovski, J. Hedberg, Y. S. Hedberg, *Biointerphases* **2021**, *16*, 021005.
- [49] E. Romanovskaia, P. Slovenský, S. M. Kalantarian, L. Laundry-Mottiar, V. Romanovski, M. Halama, M. Auinger, Y. S. Hedberg, *J. Electrochem. Soc.* **2022**, *169*, 021501.
- [50] M. Bajaj, N. Wangoo, D. V. S. Jain, R. K. Sharma, *Sci. Rep.* **2020**, *10*, 8213.
- [51] H. N. Verma, P. Singh, R. M. Chavan, *Vet. World* **2014**, *7*, 72.
- [52] J. W. Park, J. S. Shumaker-Parry, *J. Am. Chem. Soc.* **2014**, *136*, 1907.
- [53] K. P. Valente, A. Suleman, A. G. Brolo, *ACS Appl. Bio Mater.* **2020**, *3*, 6992.
- [54] H. Hinterwirth, S. K. Wiedmer, M. Moilanen, A. Lehner, G. Allmaier, T. Waitz, W. Lindner, M. Lämmerhofer, *J. Sep. Sci.* **2013**, *36*, 2952.
- [55] S. Shrestha, B. Wang, P. Dutta, *Adv. Colloid Interface Sci.* **2020**, *279*, 102162.
- [56] E. J. W. Verwey, *J. Phys. Chem.* **1947**, *51*, 631.
- [57] T. Kim, K. Lee, M. S. Gong, S. W. Joo, *Langmuir* **2005**, *21*, 9524.
- [58] Y. T. He, J. Wan, T. Tokunaga, *J. Nanopart. Res.* **2008**, *10*, 321.
- [59] Ž. Krpetić, S. Anguissola, D. Garry, P. M. Kelly, K. A. Dawson, in *Nanomaterial* (Eds: D. G. Capco, Y. Chen), Springer, Dordrecht **2014**, pp. 135–156.
- [60] C. G. Worley, R. W. Linton, *J. Vac. Sci. Technol., A* **1995**, *13*, 2281.
- [61] K. M. Harkness, L. S. Fenn, D. E. Cliffler, J. A. McLean, *Anal. Chem.* **2010**, *82*, 3061.
- [62] Y. P. Kim, E. Oh, H. K. Shon, D. W. Moon, T. G. Lee, H. S. Kim, *Appl. Surf. Sci.* **2008**, *255*, 1064.
- [63] W. R. Fawcett, M. Fedurco, Z. Kovacova, Z. Borkowska, *J. Electroanal. Chem.* **1993**, *368*, 265.
- [64] Z. Liu, H. Zhang, S. Hou, H. Ma, *Microchim. Acta* **2012**, *177*, 427.
- [65] G. Hager, A. G. Brolo, *J. Electroanal. Chem.* **2003**, *550*, 291.
- [66] T. M. Tsao, Y. M. Chen, M. K. Wang, *J. Environm. Monit.* **2011**, *13*, 1156.
- [67] L. D. Burke, P. F. Nugent, *Gold Bull* **1998**, *31*, 39.
- [68] P. Cao, N. Wang, D. Chen, S. Sun, H. Ma, M. Lin, *Gold Bull* **2021**, *54*, 97.
- [69] O. S. Ivanova, F. P. Zamborini, *Anal. Chem.* **2010**, *82*, 5844.
- [70] N. P. Finkelstein, R. D. Hancock, *Gold Bull* **1974**, *7*, 72.
- [71] Y. Ling, J. C. Elkenbracht, W. F. Flanagan, B. D. Lichter, *J. Electrochem. Soc.* **1997**, *144*, 2689.
- [72] F. Xu, F. Wang, D. Yang, Y. Gao, H. Li, *Mater. Sci. Engineer. C.* **2014**, *38*, 292.
- [73] C. Deng, J. Chen, X. Chen, M. Wang, Z. Nie, S. Yao, *Electrochim. Acta.* **2009**, *54*, 3298.
- [74] N. Spātaru, B. V. Sarada, E. Popa, D. A. Tryk, A. Fujishima, *Anal. Chem.* **2001**, *73*, 514.
- [75] M. A. MacDonald, P. Zhang, H. Qian, R. Jjin, *J. Phys. Chem. Lett.* **2010**, *1*, 1821.
- [76] P. Buffat, J.-P. Borel, *Phys. Rev. A.* **1976**, *13*, 2287.
- [77] C. C. Yang, S. Li, *Phys. Rev. B Condens Matter Mater. Phys.* **2007**, *75*, 165413.
- [78] T. Stepan, L. Tété, L. Laundry-Mottiar, E. Romanovskaia, Y. S. Hedberg, H. Danninger, M. Auinger, *Electrochim. Acta.* **2022**, *409*, 139923.
- [79] E. Gonzalez Solveyra, I. Szeleifer, *Wiley Interdiscip. Rev. Nanomed. Nanobiotechnol.* **2016**, *8*, 334.
- [80] O. S. Ivanova, F. P. Zamborini, *J. Am. Chem. Soc.* **2010**, *132*, 70.
- [81] Z. Li, Q. Fu, Y. Xue, Z. Cui, *Mater. Chem. Phys.* **2018**, *214*, 499.
- [82] M. Tagliazucchi, I. Szeleifer, *Soft Matter* **2012**, *8*, 7292.
- [83] S. R. Saptarshi, A. Duschl, A. L. Lopata, *J. Nanobiotechnol.* **2013**, *11*, 26.
- [84] M. Tambasco, S. K. Kumar, I. Szeleifer, *Langmuir* **2008**, *24*, 8448.
- [85] J. A. Carr, H. Wang, A. Abraham, T. Gullion, J. P. Lewis, *J. Phys. Chem. C* **2012**, *116*, 25816.
- [86] S. Maheshwari, Y. Li, M. J. Janik, *J. Electrochem. Soc.* **2022**, *169*, 064513.
- [87] G. Gritzner, M. Auinger, *Acta Chim. Slov.* **2009**, *56*, 86.
- [88] B. Pem, M. Toma, V. Vrček, I. Vinković Vrček, *Inorg. Chem.* **2021**, *60*, 4144.
- [89] M. P. Seah, A. G. Shard, *Appl. Surf. Sci.* **2018**, *439*, 605.
- [90] T. L. Colliver, C. L. Brummel, M. L. Pacholski, F. D. Swanek, A. G. Ewing, N. Winograd, *Anal. Chem.* **1997**, *69*, 2225.
- [91] W. Wei, J. Xu, W. Chen, L. Mi, J. Zhang, *J. Mater. Chem. A Mater.* **2022**, *10*, 2637.
- [92] B. Ravel, M. Newville, *J. Synchrotron Radiat.* **2005**, *12*, 537.
- [93] W. R. Fawcett, M. Fedurco, Z. Kováčová, Z. Borkowska, *J. Electroanal. Chem.* **1994**, *368*, 275.